Controlled mode tuning in 1-D 'RIM' plasmonic crystal trench cavities probed with coupled optical emitters

Controlled mode tuning in 1-D 'RIM' plasmonic crystal trench cavities probed with coupled optical emitters

Tsung-li Liu,* Kasey J. Russell, Shanying Cui, and Evelyn L. Hu

School of Engineering and Applied Science, Harvard University, Cambridge, Massachusetts, 02138, USA
**tlliu@fas.harvard.edu*

Abstract: We present a design of plasmonic cavities that consists of two sets of 1-D plasmonic crystal reflectors on a plasmonic trench waveguide. A 'reverse image mold' (RIM) technique was developed to pattern high-resolution silver trenches and to embed emitters at the cavity field maximum, and FDTD simulations were performed to analyze the frequency response of the fabricated devices. Distinct cavity modes were observed from the photoluminescence spectra of the organic dye embedded within these cavities. The cavity geometry facilitates tuning of the modes through a change in cavity dimensions. Both the design and the fabrication technique presented could be extended to making trench waveguide-based plasmonic devices and circuits.

OCIS codes: (250.0250) Optoelectronics; (250.5403) Plasmonics.

References and links

1. K. J. Vahala, "Optical microcavities," Nature **424**(6950), 839–846 (2003).
2. P. Goy, J. M. Raimond, M. Gross, and S. Haroche, "Observation of cavity-enhanced single-atom spontaneous emission," Phys. Rev. Lett. **50**(24), 1903–1906 (1983).
3. K. Hennessy, A. Badolato, M. Winger, D. Gerace, M. Atatüre, S. Gulde, S. Fält, E. L. Hu, and A. Imamoğlu, "Quantum nature of a strongly coupled single quantum dot-cavity system," Nature **445**(7130), 896–899 (2007).
4. S. Kühn, U. Håkanson, L. Rogobete, and V. Sandoghdar, "Enhancement of single-molecule fluorescence using a gold nanoparticle as an optical nanoantenna," Phys. Rev. Lett. **97**(1), 017402 (2006).
5. R. F. Oulton, V. J. Sorger, T. Zentgraf, R. M. Ma, C. Gladden, L. Dai, G. Bartal, and X. Zhang, "Plasmon lasers at deep subwavelength scale," Nature **461**(7264), 629–632 (2009).
6. K. J. Russell, T.-L. Liu, S. Cui, and E. L. Hu, "Large spontaneous emission enhancement in plasmonic nanocavities," Nat. Photonics **6**(7), 459–462 (2012).
7. P. Mühlschlegel, H.-J. Eisler, O. J. F. Martin, B. Hecht, and D. W. Pohl, "Resonant optical antennas," Science **308**(5728), 1607–1609 (2005).
8. J. Dintinger, S. Klein, F. Bustos, W. L. Barnes, and T. W. Ebbesen, "Strong coupling between surface plasmon-polaritons and organic molecules in subwavelength hole arrays," Phys. Rev. B **71**(3), 035424 (2005).
9. P. Anger, P. Bharadwaj, and L. Novotny, "Enhancement and quenching of single-molecule fluorescence," Phys. Rev. Lett. **96**(11), 113002 (2006).
10. K. Okamoto, I. Niki, A. Shvartser, Y. Narukawa, T. Mukai, and A. Scherer, "Surface-plasmon-enhanced light emitters based on InGaN quantum wells," Nat. Mater. **3**(9), 601–605 (2004).
11. D. E. Chang, A. S. Sørensen, P. R. Hemmer, and M. D. Lukin, "Quantum optics with surface plasmons," Phys. Rev. Lett. **97**(5), 053002 (2006).
12. H. Rigneault, J. Capoulade, J. Dintinger, J. Wenger, N. Bonod, E. Popov, T. W. Ebbesen, and P.-F. Lenne, "Enhancement of single-molecule fluorescence detection in subwavelength apertures," Phys. Rev. Lett. **95**(11), 117401 (2005).
13. S. I. Bozhevolnyi, V. S. Volkov, E. Devaux, and T. W. Ebbesen, "Channel plasmon-polariton guiding by subwavelength metal grooves," Phys. Rev. Lett. **95**(4), 046802 (2005).
14. E. J. Vesseur, F. J. García de Abajo, and A. Polman, "Modal decomposition of surface--plasmon whispering gallery resonators," Nano Lett. **9**(9), 3147–3150 (2009).
15. C. L. C. Smith, B. Desiatov, I. Goykmann, I. Fernandez-Cuesta, U. Levy, and A. Kristensen, "Plasmonic V-groove waveguides with Bragg grating filters via nanoimprint lithography," Opt. Express **20**(5), 5696–5706 (2012).
16. E. J. R. Vesseur and A. Polman, "Controlled spontaneous emission in plasmonic whispering gallery antennas," Appl. Phys. Lett. **99**(23), 231112 (2011).
17. P. Nagpal, N. C. Lindquist, S.-H. Oh, and D. J. Norris, "Ultrasmooth patterned metals for plasmonics and metamaterials," Science **325**(5940), 594–597 (2009).

#199181 - $15.00 USD Received 10 Oct 2013; revised 16 Nov 2013; accepted 18 Nov 2013; published 27 Nov 2013

18. M. J. Loboda and G. A. Toskey, "Understanding hydrogen silsesquioxane-based dielectric films processing," Solid State Technol. **41**, 5 (1998).
19. A. Polyakov, H. A. Padmore, X. Liang, S. Dhuey, B. Harteneck, J. P. Schuck, and S. Cabrini, "Light trapping in plasmonic nanocavities on metal surfaces," J. Vac. Sci. Technol. B **29**(6), 06FF01 (2011).
20. Y. Akahane, T. Asano, B.-S. Song, and S. Noda, "High-Q photonic nanocavity in a two-dimensional photonic crystal," Nature **425**(6961), 944–947 (2003).
21. K. J. Russell, K. Y.-M. Yeung, and E. L. Hu, "Measuring the Mode volume of plasmonic nanocavities using coupled optical emitters," Phys. Rev. B **85**(24), 245445 (2012).
22. S. Zhang, Y.-S. Park, Y.-M. Liu, T. Zentgraf, and X. Zhang, "Far-field measurement of ultra-small plasmonic mode volume," Opt. Express **18**(6), 6048–6055 (2010).
23. Y. Guo, L. Yan, W. Pan, B. Luo, K. Wen, Z. Guo, H. Li, and X. Luo, "A plasmonic splitter based on slot cavity," Opt. Express **19**(15), 13831–13838 (2011).
24. Y. Guo, L. Yan, W. Pan, B. Luo, K. Wen, Z. Guo, and X. Luo, "Characteristics of plasmonic filters with a notch located along rectangular resonators," Plasmonics **8**(2), 167–171 (2013).

1. Introduction

Confining light to near-wavelength or sub-wavelength dimensions using optical microcavities makes possible many applications in quantum photonics. The creation of well-defined resonant cavity modes enables selective enhancement of light-matter interactions both spatially and spectrally. Such selective enhancement in turn allows the deterministic observation of phenomena including enhanced spontaneous emission, ultra-low threshold lasing and strong coupling between photonic and electronic states [1–3]. Many of these phenomena and many of the breakthroughs for optical cavities have been realized in dielectric materials. However, there has been recent progress in, and excitement about, metal-based optical cavities, where much smaller mode volumes can be achieved [4–10]. These developments have opened up applications of metal cavities in light emission, quantum optics and optical sensing [10–12].

Despite the significant progress that has been made in the formation of these 'plasmonic' cavities, there is much room for improvement to ensure well-controlled dimensions to produce the desired modes, to optimally integrate and couple the emitter to the cavity, and to further scale the device geometry to allow cavity-cavity interactions. In this paper, we introduce a cavity formed from a narrow trench on a silver surface. We will discuss both the predicted optical properties of the device as simulated by finite difference time domain (FDTD) simulations as well as experimental results.

Narrow trench structures have been previously identified as excellent candidates for plasmonic waveguides with highly concentrated fields [13–15]. Similar to the way in which dielectric cavities can be created from dielectric waveguides with different reflective terminations (e.g. photonic crystals and ring resonators), various plasmonic cavity designs have been realized by different ways of terminating metallic trench waveguides.

In this work, we propose to use periodic modulations of the width of metallic trenches as periodic reflectors (1-D photonic crystals) to form plasmonic cavities. This design allows us to tune the cavity confinement by adjusting the number of periods of the modulation. This geometry also allows us to control coupling between the cavity and the adjacent regions of trench waveguide, enabling cavity-waveguide and cavity-cavity coupling.

2. Design and fabrication

A schematic view of the structure is shown in Fig. 1. The proposed device consists of a trench cavity of length L and periodic modulations of the trench width at each end of the cavity, which serve as mirrors to confine electromagnetic energy within the cavity region. The devices presented in this article have periodic modulations with pitches ranging from a = 400nm to 500nm; a cavity length L = 2a; and a constant modulation length d = 150nm. The definition of all these parameters can be found in Fig. 1(a). The trench depths, h_1 for the wider portion and h_2 for the narrower portion, are determined by the fabrication process, which will be described in following paragraphs. The metallic material chosen in this work is silver, which has been demonstrated to be a good plasmonic material for most of the visible frequency range.

#199181 - $15.00 USD Received 10 Oct 2013; revised 16 Nov 2013; accepted 18 Nov 2013; published 27 Nov 2013

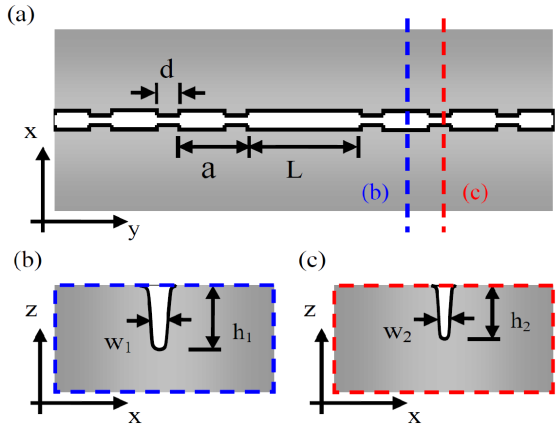

Fig. 1. Schematic cartoon of the trench cavity: (a) a top-down view, (b) a cross-section view of the wider part of the trench (blue dashed line in (a)) and (c) a cross-section view of the narrower part of the trench (red dashed line in (a)). For the actual working device, w_1, w_2, h_1, h_2 were measured by SEM to be approximately 30, 15, 150, 110 nm, respectively.

A straightforward way of fabricating such structures is to use focused ion beam (FIB) milling to create the trenches directly into metal substrates [13, 14]. However, with FIB milling, the width of the trench is limited by the finite ion beam size (15 – 50 nm, depending on the FIB current), and the smoothness of the metallic sidewalls is limited by the sputtering process. In addition, there is unavoidable ion implantation by the beam into the remaining metal that, in our experience, greatly increases the absorptive loss of the resulting devices. Furthermore, there are challenges in placing optically active materials at the bottom of a very narrow metal trench, where the intensity of the cavity modes is highest [14, 16].

We have therefore adopted a different fabrication approach. A high-spatial resolution 'reverse image mold' (RIM) was first formed using electron beam lithography, and then the metal cavity was formed around the mold using a version of template-stripping [17]. A schematic diagram of the process is shown in Fig. 2. A layer of XR 1541 electron-beam (E-beam) resist, 150 nm thick, was deposited on top of an oxidized Si wafer. XR 1541 is a high resolution negative resist that is converted into a silicon-containing dielectric material under electron beam irradiation with a 100kV Elionix F-7000 e-beam lithography system with a 2200μC/cm^2 dosage [18]. The result of this lithography step is a set of 150 nm tall dielectric ridges, as shown in Figs. 3(a) and 3(b). These dimensions will define the width and depth of the trench cavities.

These dielectric ridges serve as the 'reverse image molds' or templates for our metallic trench cavities. We subsequently deposited 5 nm of organic molecular emitter tris(8-hydroxyquinolinato)aluminium (Alq_3) onto the template by thermal evaporation and then sputter-coated a 2 nm Al_2O_3 protective layer and 500 nm of silver. The silver layer will serve as the actual cavity. Pieces of a silicon wafer were then anchored onto the silver surface with epoxy (EPO-TEK 377, Epoxy Technologies), which was cured at 150°C for 3 hours. The fabricated metallic cavities were removed from the templates by sliding the blade of a razor under the edge of the silicon. This modification of a 'template stripping' process [17, 19] enables the interior walls of the silver trench to be nearly as smooth as the exterior surface of the dielectric ridge coated in Alq_3 and Al_2O_3.

#199181 - $15.00 USD Received 10 Oct 2013; revised 16 Nov 2013; accepted 18 Nov 2013; published 27 Nov 2013

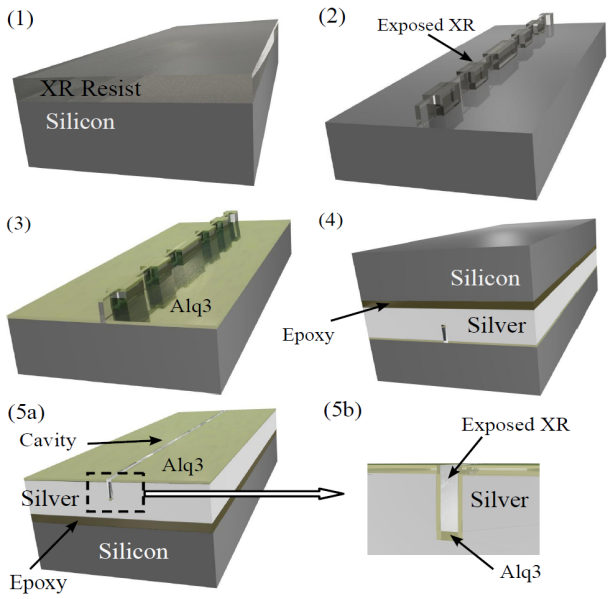

Fig. 2. Process flow for fabricating template-stripped trench cavities. Step (1): spin coat XR-1541 onto a clean, smooth silicon wafer. Step (2): pattern XR with e-beam lithography. Step (3): evaporate 5nm of Alq3 upon the template. Step (4): sputter -coat 500nm of silver onto the template, and attach the exposed surface of the silver layer to a wafer piece using epoxy. Step (5a): peel off the original silicon substrate and flip the chip over. Step (5b) cross-section view of the final trench. (Region enclosed by the dashed line in step (5a)).

A top-down scanning electron microscope (SEM) image of a fabricated trench cavity is shown in Fig. 3(c). An important feature of this process is apparent from the schematic view of the cavity cross section, shown in Fig. 2 (Step 5b): the organic emitter, Alq_3, is embedded within the trench, co-located with the highly concentrated field of the cavity. This ensures good overlap of the emitters with the cavity modes as we will show in the simulated field distribution later in this article.

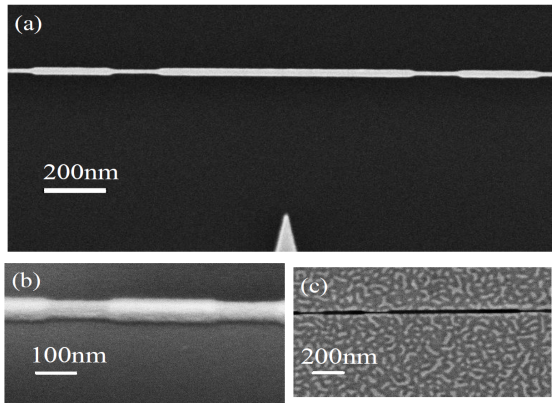

Fig. 3. SEM images of: (a) top-down view of the RIM, (b) 40° angled view of the RIM and (c) top-down view of the fabricated trench

3. Simulation and measurement results

In order to evaluate the effectiveness of this device as a plasmonic cavity, we performed finite difference time domain (FDTD) simulations with *FDTD Solutions* (Lumerical Inc.). According to the SEM images (Fig. 3(a)), the RIM has rounded edges, and spectroscopic

#199181 - $15.00 USD Received 10 Oct 2013; revised 16 Nov 2013; accepted 18 Nov 2013; published 27 Nov 2013

ellipsometry done on an XR-1541 film indicate that it has a refractive index of ~1.4. The wider segment of the RIM (schematic in Fig. 1(b)) is ~30nm wide and ~150nm tall, as defined by the thickness of the initial resist film. However, the more narrow segment (schematic in Fig. 1(c)), which is about 15nm wide, has a height of ~110nm, lower than the original resist thickness. This indicates that only the part of the resist closest to the substrate is sufficiently exposed during the e-beam lithography, suggesting that the incident electron beam alone is insufficient to fully expose the resist without additional exposure from electron back-scattering from the substrate. At the small lateral dimensions desired for our trench structures, the resist profile is very sensitive to the electron dose. We believe that there are ways to mitigate this sensitivity, but the devices described here incorporate a variation in both width and depth. The dimensions we provide here are based on the devices that worked the best among all the devices fabricated with various electron doses.

The structure was simulated according to parameters measured from the actual devices. In the simulation, an electric oscillating dipole source is placed into the center of the trench, 30nm above bottom of the trench. In order to couple well to the surface plasmon mode which has a primary electric field perpendicular to the metal surface, the dipole should be oriented perpendicular to the trench (x-direction in Fig. 1(a)). In our simulation, it is oriented along the x-axis with a small tilt of 15 degrees clockwise in the x-y plane. The small tilt slightly reduces coupling efficiency but was used to verify that there are no modes with electric field parallel to the metal surface. This dipole generates a short electrical pulse (~15 fs duration) at the beginning of the simulation and the Fourier transform of such a short pulse results in a broadband spectral distribution of the generated radiation ranging from ~500 to 700 nm in wavelength. The simulation calculates the total field response to the dipole emission for 300 fs. The electric field intensity was then recorded and the frequency response of the device can be analyzed by the Fourier transform of the time-dependent electric field intensity.

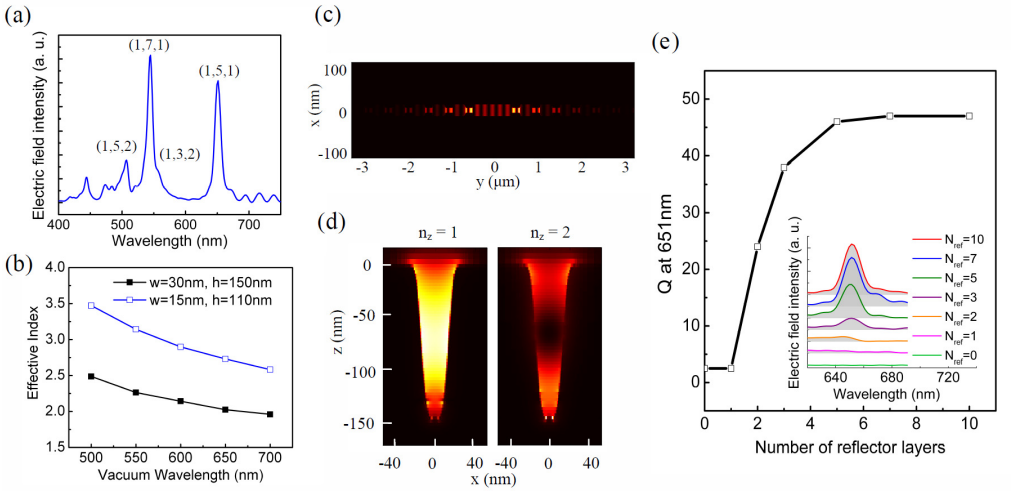

Fig. 4. FDTD simulation on trench cavities including: (a) the simulated spectrum of a cavity with reflector periodicity of a = 425nm, (b) effective index of the fundamental waveguide mode (n_x = n_z = 1) in the trenches with various dimensions, (c) in-plane electric field distribution recorded by a monitor 70nm below the top metal surface, (d) cross-sectional electric field distribution for modes with n_z = 1 and n_z = 2 and (e) Q and mode spectra dependence on number of reflector layers for the (1,5,1) mode.

The simulated spectrum is shown in Fig. 4(a). Several sharp peaks corresponding to cavity resonances can be seen in the figure. The quality factors (Qs) of these resonances can be estimated from the linewidths of these peaks to be ~30-50. To identify these transitions as resonant modes in terms of their quantum numbers (n_x, n_y, n_z) in each dimension in the cavity, a series of FDTD simulations was performed to extract the effective index of the waveguide modes in the trench waveguide. Figure 4(b) shows the simulated effective index for the

#199181 - $15.00 USD Received 10 Oct 2013; revised 16 Nov 2013; accepted 18 Nov 2013; published 27 Nov 2013

fundamental waveguide mode ($n_x = n_z = 1$) with wavelengths from 500 to 700nm. The wavelength of the cavity modes can then be predicted with a simplified model as:

$$L = \frac{n_y}{2}\frac{\lambda}{n_{eff}}, \quad (1)$$

where L = 850nm is the cavity length as defined in Fig. 1(a), and n_{eff} is the effective index. This model ignores the phase shift due to reflection at the periodic mirrors but can still help us to estimate resonant wavelengths of the cavity modes. The analysis suggested that only two modes, (n_x, n_y, n_z) = (1, 5, 1) and (1, 7, 1), lie within the spectral range of interest. The vacuum wavelengths (λ) were predicted as $\lambda_{(1,5,1)}$ = 662nm and $\lambda_{(1,7,1)}$ = 551nm, agree fairly well with the wavelengths of the two major peaks in the simulated spectrum. The quantum numbers are labeled in Fig. 4(a) above each peak; the axes are defined as previously shown in Fig. 1(a). Besides the two modes predicted by our analysis, there are also some lower intensity transitions observed in the spectrum. Comparing the spectrum with the frequency-dependent electric field distribution allows us both to further confirm our calculation of the two modes and to identify the other transitions as resonances from higher order waveguide modes. Since the width of the trench is much less than half of the effective wavelength, only the fundamental mode in the x direction is supported. In the z direction, two orders of modes are observed, limited by the trench depth. The electric field distributions of the two modes are shown in Fig. 4(d) (similar to mode number n = 1, 2 in [14]).

Figure 4(c) and the left panel of (d) show the top-down and cross-sectional views, respectively, of the field distribution of the (1, 5, 1) mode at 651 nm. A few observations should be made. First, the cross-sectional view shows strong field intensity deep inside the trench. Thus, this geometry is capable of concentrating the field into a 10^{-4} $(1/\lambda)^2$ cross-sectional area. Second, the major electric field component is polarized in the x direction (across the trench). The polarization will be used to compare with the measurement results later in this article. Lastly, the field travels within the trench waveguides and is reflected by the mirrors, showing a Fabry-Perot like interference pattern along the y axis as seen in Fig. 4(c).

In order to understand how the morphology of the periodic modulations affected the cavity confinement characteristics, a series of simulations were performed. We varied the number of modulations (N_{ref} in Fig. 4(e)) in each side and monitored the change of cavity Q. The dependence of Q of the (1,5,1) mode on numbers of modulations (N_{ref}) is shown in Fig. 4(e). The quality factor of the mode plateaus at Q ~46 at N_{ref} greater than 5. A clear decrease in Q can be seen when N_{ref} decreases, and the resonance is not well defined when $N_{ref} < 1$. These results demonstrate that the modulations do help in confining the field and we can control the confinement of the cavity by adjusting the number of modulations. There are some limitations to the confinement strength. First, the strong propagation loss in such a tightly confined plasmonic waveguide prevents long distance interference between the reflected waves. This fact is a principal limitation to the performance of the device. Second, the same observation indicates that we need sufficient reflection from *each* modulation to provide enough confinement over the field. This will result in higher mode mismatch and greater scattering loss at each reflective interface, also limiting the Q of the cavities. (A similar issue pertains to dielectric cavities, as discussed by S. Noda et al. in 2003 [20], but the relative impact for these metal structures is far more severe because of their larger propagation losses).

The devices fabricated for measurement were a series of trench cavities with various dimensions in the trench axis (y axis in Fig. 1). Trench cavities with lattice constant a = 425, 450, 475 and 500nm were made simultaneously. The fabricated structure was characterized with micro-photoluminescence measurements. A temporally pulsed beam at a wavelength of 455nm from a frequency-doubled Ti:Sapphire laser system was directed through a 100x, 0.9 numerical aperture objective onto the trench cavities containing Alq_3. Luminescence from the

#199181 - $15.00 USD Received 10 Oct 2013; revised 16 Nov 2013; accepted 18 Nov 2013; published 27 Nov 2013

excited molecules was then collected by the same objective. The collected signal was analyzed by a grating spectrometer with liquid-nitrogen cooled CCD array.

As shown in Fig. 5(a), the excited Alq_3 on the unpatterned metal surface gives a broadband fluorescence spectrum over 500-700nm (off-cavity trace in Fig. 5(a)). By comparison, the fluorescence spectrum of Alq_3 embedded in the trench cavity is strongly modified by the cavity structure (on-cavity traces in Fig. 5(a)). Distinct cavity modes with quality factors ranging from 40 to 60 are observed. These resonant modes are polarized in the x direction, perpendicular to the trench direction, as is the far field scattering toward positive z direction, which is collected by the objective. Therefore, as shown in Fig. 5(b), by using the polarization of the PL spectrum, we can isolate the emission associated with molecules coupled to the trench plasmonic modes from random spontaneous emission. By comparing the integrated intensity of the parallel (y-direction) and cross (x-direction) polarized signals, we conclude that over 90 percent of the total signal is from photons coupled to the guiding modes in the trench.

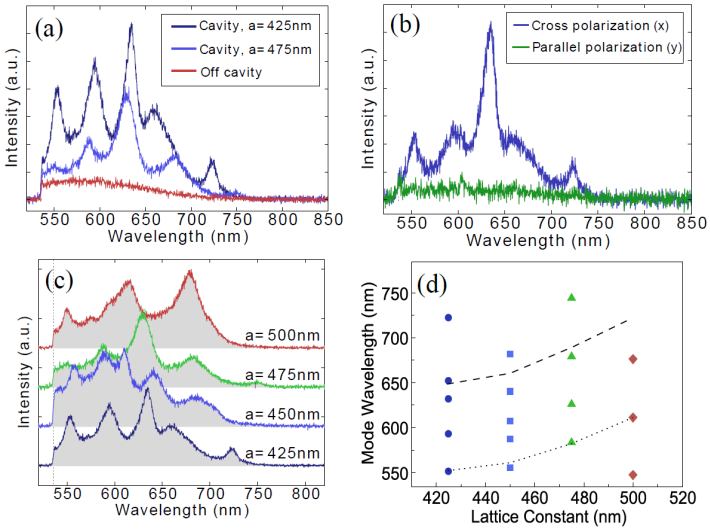

Fig. 5. (a) Photoluminescence (PL) spectra measured on and off cavities. (b) Polarization dependence of PL spectrum of a trench cavity. (c) Normalized PL spectra of trench cavities with various grating pitches and (d) dependence of resonant wavelengths on lattice constant. The dashed line indicates simulated peak wavelength of the (1,5,1) mode and the dotted line indicates the (1,7,1) mode. All spectra were taken under an excitation power of 7μw (~900w/cm^2) and integrated for 20 seconds.

Figure 5(c) shows PL spectra from trench cavities with various lattice constants (a = 425 nm – 500 nm). A clear shift of the cavity modes is observed for different cavity dimensions. Tracking the mode wavelength with the pitch of the plasmonic cavity, as shown in Fig. 5(d), indicates that the resonant condition scales with the pitch of the cavities. The various colored points are the mode positions for the devices at different values of lattice constant. The dashed and dotted lines in the figure are the simulated values for (1, 5, 1) and (1, 7, 1) modes. The measured shifts with lattice constant show a similar trend as the simulated values, particularly for the lower wavelength modes, but there are more modes observed in the measured spectra. The excess modes are due to the fact that in real devices the emitters are distributed uniformly all over the trench sidewalls, not only at the center of the cavity regions as in the simulation. The capability to deterministically shift the cavity mode enables spectrally selective enhancement of the emission of the organic dye. This would be useful, for example, to study the difference in plasmon-matter interaction of molecules in and out of resonance with the cavity mode, as has been demonstrated in dielectric optical microcavities [3]. In plasmonic structures, such deterministic control over low Q (broadband) resonances

#199181 - $15.00 USD Received 10 Oct 2013; revised 16 Nov 2013; accepted 18 Nov 2013; published 27 Nov 2013

has been shown, and continuous tuning of non-deterministic high Q resonances has been achieved [21–24]. However, the low Q and/or non-deterministic nature of these previous works limited their application results in limited applicability to cQED studies. In addition, since the cavity design presented here builds upon a trench waveguide, there is a natural way to join cavities to waveguides to couple together spatially separate cavities.

4. Conclusions

In conclusion, we have demonstrated a cavity design which can be lithographically patterned to provide plasmonic resonators with tuned resonances. We have developed a reverse image mold (RIM) technique to fabricate these cavities that allows us exceptional control over the orientation and dimensions of the resulting devices. The method enables incorporation of evaporated organic dyes to be inserted into the field maximum of the cavities, allowing us to probe the cavity characteristics using the luminescence spectrum of the dye.

FDTD simulations of these cavities show promising resonances with Q of approximately 30-50 and modal volumes of $\sim 3 \times 10^{-2}$ $(\lambda/n)^3$. Experimental values of Q, determined from emission spectra of the embedded fluorescent dye molecules, are comparable to simulation values, and the mode resonance frequencies shift controllably in response to changes in the geometry of the cavities.

These results demonstrate a robust, controlled method for fabricating high-confinement metal-based optical cavities. This approach could enable high-confinement metallic optical cavities to be integrated into waveguide devices.

Acknowledgments

We gratefully acknowledge financial support from the NSF Nanoscale Science and Engineering Center under Grant No. NSF/PHY-06-46094, the use of the NSF National Nanotechnology Infrastructure Network facilities at Harvard University's Center for Nanoscale Systems, the assistance of staff members in Harvard University's Center for Nanoscale Systems and the use of the high-performance computing computer cluster at Harvard.

#199181 - $15.00 USD Received 10 Oct 2013; revised 16 Nov 2013; accepted 18 Nov 2013; published 27 Nov 2013